Chapter 1

Bismuth Ferrites/Graphene Nanoplatelets Nanohybrids for Efficient Organic Dye Removal

Syed Rizwan and Sabeen Fatima

Additional information is available at the end of the chapter

http://dx.doi.org/10.5772/intechopen.75807

Abstract

The doped bismuth ferrites have got tremendous attraction owing to its ideal properties for photocatalysis application. We have fabricated the novel lanthanum and manganese co-doped $BiFeO_3$ (namely BLFMO)/graphene nanoplatelets (GNPs) nanohybrid for photocatalysis with easy and effective synthesis routes namely the co-precipitation (C-hybrid) and hydrothermal (H-hybrid) processes. The H-hybrid showed crystalline structure with lower band-gap than the C-hybrid samples. However, C-hybrid showed higher dye degradation (92%) due its higher surface area (55 m^2/g) and the fine incorporation of BLFMO nanoparticles into the GNPs which enhanced the surface adsorption. This is verified from more degradation in dark conditions for these samples. The proposed nanohybrids are novel for photocatalytic application fabricated through the low cost routes which show higher efficiency for practical applications.

Keywords: graphene nanoplatelets, nanohybrid, photocatalysis, co-precipitation, adsorption

1. Introduction

1.1. Bismuth ferrite

Bismuth ferrite $BiFeO_3$ also called BFO is the only naturally existing magnetoelectric materials. BFO possess a perovskite structure with ABO_3 type atoms where A and B represent the cations and O is the oxygen atoms or anions. A are corner atoms, B are the body centered and O are the atoms attach to the faces of the unit cell as shown in **Figure 1**.

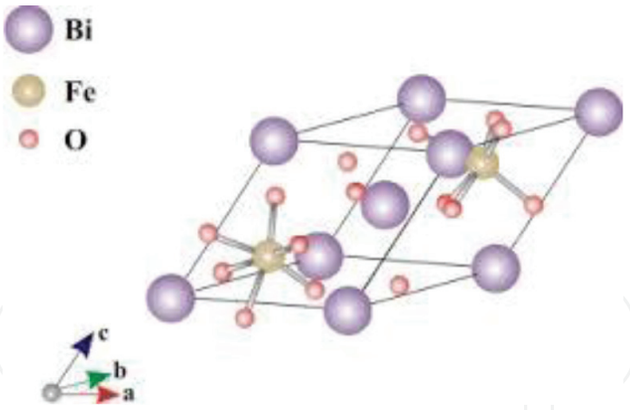

Figure 1. Perovskite structure [1].

The perovskite structures are of great interest due to their magnetic, multiferroic and photocatalytic properties. These properties are beneficial for different applications such as in non-volatile memories [2], photochemical cells [3], thin films capacitors [4] and non-linear optics [5]. Perhaps BFO is the only perovskite material representing both strong ferroelectric and magnetic effect at room temperature [6]. The BFO is doped with various elements due to which its structural, electrical and magnetic properties are improved. This enhancement in properties provides a great use of doped BFO particles in different industrial and medical applications.

1.2. Carbon-based 2D materials

Carbon is an important element of our nature and is approximately present in all living forms. In nature carbon is available in many allotropic forms with different chemical and physical properties. Important crystalline forms of carbon are fullerene (0D), carbon nanotube (2D), graphene (2D), graphite and diamond (3D).

1.2.1. Graphene

Graphene is a two dimensional (2D) allotrope of carbon in which carbon atoms are hexagonally arranged in a single layer pattern. Graphene being lighter in weight, flexible and strongest material is getting more popular day by day. In these years graphene spell has

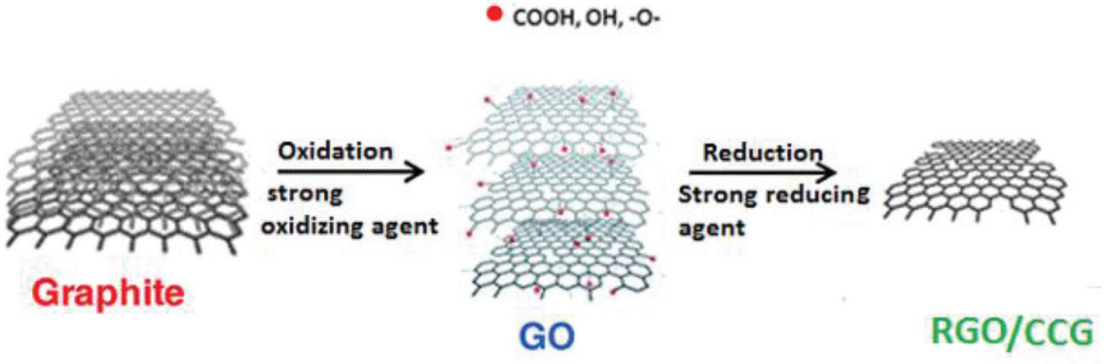

Figure 2. Chemically converted graphene by chemical exfoliation [10].

covered the complete industry and due to its extraordinary optical [7], mechanical, electronic and magnetic properties [8] it is considered to be the most important material for whole optical and electronic media. Single layer graphene is unstable and is difficult to prepare. The first stable single layer of graphene was made by Geim and Novoselov [9]. The easiest and cheapest way to synthesize graphene is its chemical exfoliation in which graphite is used as the starting material. By oxidation and reduction of graphite with the help of suitable oxidizing and reducing agents we reached to multilayer graphene called chemically converted graphene (CCG) or reduced graphene oxide (rGO) as shown in **Figure 2**.

1.2.2. Graphene nanoplatelets

Nanoplatelets are particles in platelet form at nanoscale. Different functional groups like carboxyls, hydroxyls or ethers are naturally attached to the edges of nanoparticles and the wt% of these group varies as the particle size is changed [11]. Graphene nanoplatelets (GNP's) are a few disk shaped round graphene sheets stacked (more than 10 layers). together as shown in **Figure 3**.

Actually GNP's are the flakes of graphene so called the GNF's. It is difficult to make GNP's even during the artificial synthesis process. So, if GNF's are not round they are still marked as graphene nanoplatelets. They have a thin but wide aspect ratio (ranging in thousand). Sometimes, the GNP's are also called graphite nanoplatelets when there are more stacked layers (about 38 layers [13]). GNP's are easy to prepare as there is no separate need of reduction. They have better conductivity with less defects. At the nanoscale GNPs are prepared by thermal exfoliation of naturally available graphite flakes [14]. Commercially, graphene nanoplatelets xGNPs (shown in **Figure 4**) are prepared with the help of intercalation process of graphite with acids, metal ions or different alkali metals with thicknesses of 1–15 nm [14].

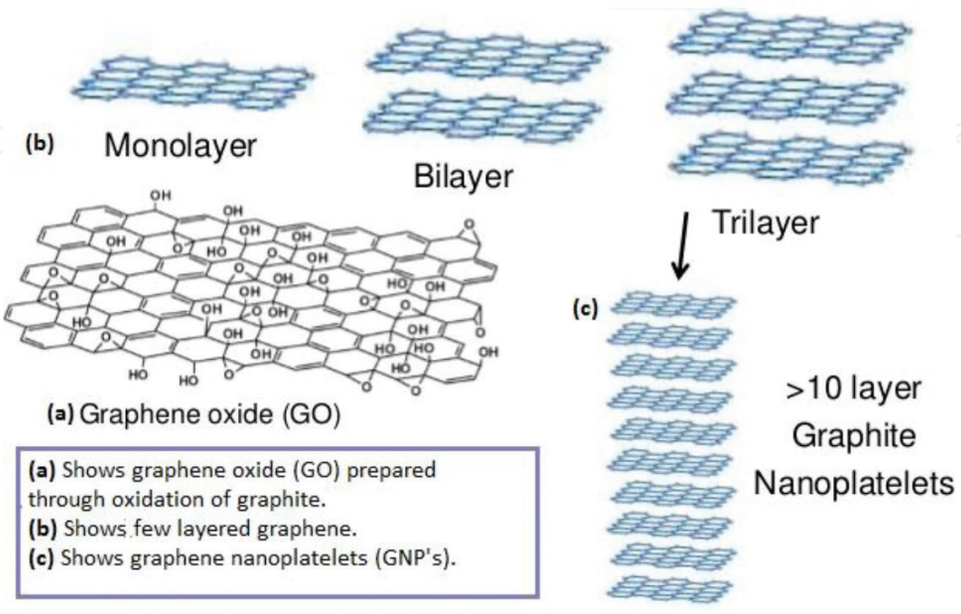

Figure 3. Difference in between GO, graphene and GNP's [12].

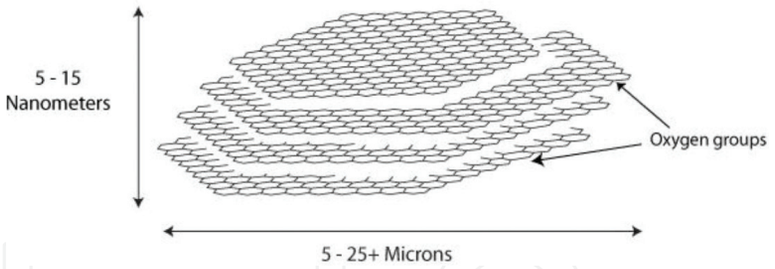

Figure 4. A typical graphene nanoplatelets (xGNPs) [15].

1.2.3. Graphene-based nanocomposites

A nanocomposite is a blend of two materials in such a way so that we can get the best properties of these materials. A nanocomposite is a hybrid structure of any two materials and among these each of these materials should have its dimension in nanoscale (less than 100 nm) [16]. It is a multiphase material in which one phase consists of a matrix while the other one is a discontinuous or reinforcing phase (usually in the form of sheets, particles or fibers). Nanocomposite materials are emerging as a suitable alternative for overcoming all the limitations which are faced by microcomposites in different applications.

Graphene nanocomposites are common and simplest hybrid structures which are prepared by adding its small amount to polymers, ceramics or metals [13]. These nanocomposites will be much stronger, heat resistive and conductive due to the addition of graphene. By combining graphene nanoplatelets with a material in a hybrid, one can improve the composite stiffness, abrasion resistance, tensile strength, corrosion resistance and lubricant properties. The nanocomposites of GNP's with other materials help in modifying the mechanical properties and conductivity of the hybrid structures.

In combination of graphene and graphene nanoplatelets in a composite form with different magnetic materials or ferrites, one can use these hybrid structures into different applications like band gap engineering, sensors, desorption, antibacterial activity, oil spilling, photocatalytic activity etc [17].

1.3. Photocatalytic activity

Photocatalytic activity involves the degradation of the pollutants present in water with the help of suitable photocatalysts. In start semiconductor oxides like ZnO, SnO_2 and TiO_2 were used as good photocatalysts due to their higher catalytic activity, excellent ultra violet (UV) absorbency, low cost, chemical stability and non-toxicity [18]. Photocatalysts perform their action by oxidizing the organic pollutants or molecules under UV light and result in carbon dioxide (CO_2) and water (H_2O) as by-products. In TiO_2, the recombination rate of photo-generated charge carriers were found to be fast and hence, making it a less efficient photocatalyst [19, 20]. Since, the solar energy is available as an abundant natural source of electromagnetic radiation and most of it consists of visible light, the best way is to use it in purification of water and hence, to find a photocatalyst that can work efficiently in the presence of visible light. Recently, it has been investigated that BFO also responses actively under visible light. BFO nanoparticles represent a significant photocatalytic activity due

to stability of crystal structure, large surface area and small energy bandgap [21]. It is possible to degrade the organic molecules within a short period of time by preparing the particles with smaller diameters or larger surfaces. The separation between electrons and holes plays a vital role in this oxidation process and hence, in photocatalysis. If this separation cannot be maintained, charge carriers will recombine resulting in no oxidation. Graphene in a hybrid structure with BFO gives an efficient way of enhancing photocatalytic activity by promoting the separation between the photo-generated pairs of electrons and holes [22, 23]. Hence, the thirst for searching new graphene-based hybrid nanocomposites with large surface area and small energy band-gap is an ever-demanding field of research.

2. Material synthesis

The material synthesis scheme for pure Bismuth ferrites, and its composites are shown in **Figures 5–7**, respectively. The visual changes occur during the hybrid preparation in co-ppt and hydrothermal synthesis are shown in the given **Figure 8**.

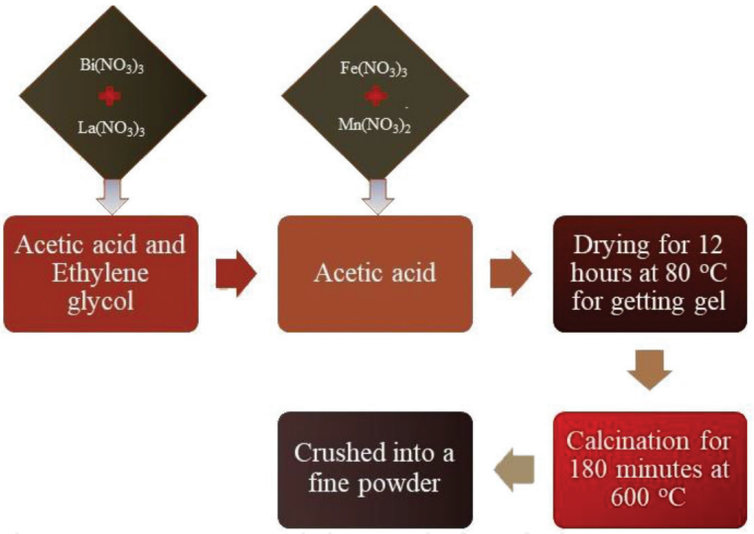

Figure 5. Sol–gel synthesis of BLFO and BLFMO nanoparticles.

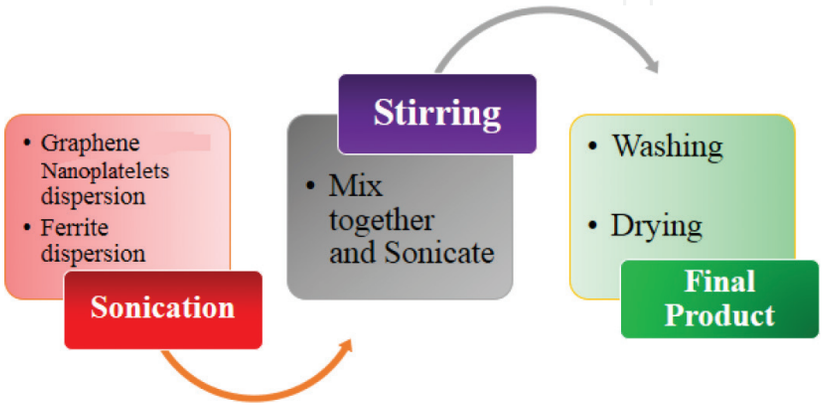

Figure 6. Ferrite-GO/GNP hybrids through Co-ppt method.

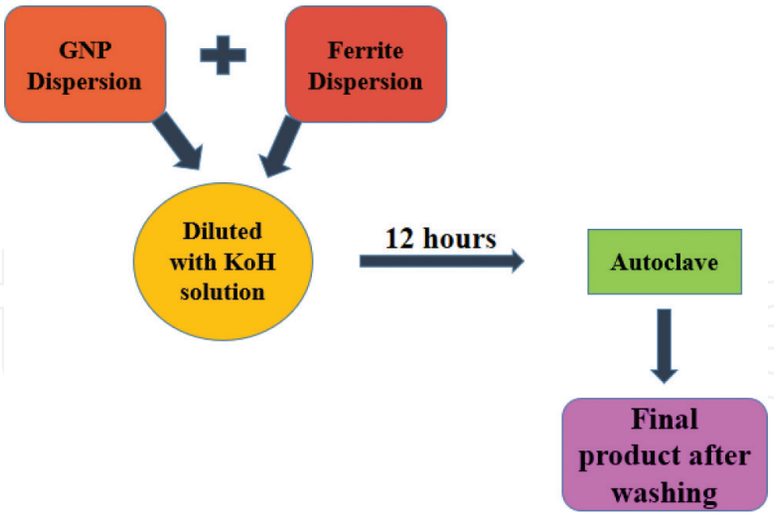

Figure 7. Hydrothermal synthesis of BLFMO/GNP nanohybrids.

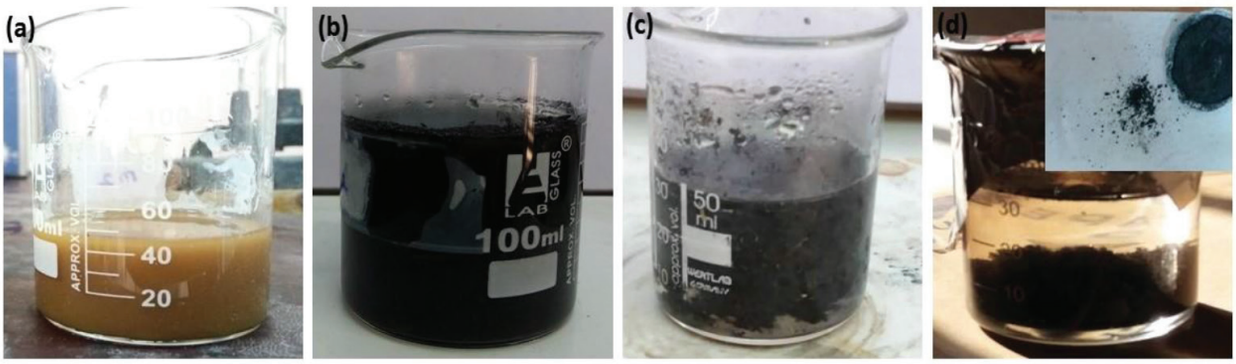

Figure 8. (a) Ferrite dispersion, (b) GNP dispersion, (c) hybrid formation, (d) sedimentation; the inset is the final dried form of hybrid structure.

3. Enhanced catalytic activity of La, Mn co-doped $BiFeO_3$/GNP nanohybrids

3.1. C-series structural analysis

The x-ray diffraction pattern was obtained by irradiating Cu-Kα rays (λ = 1.54 nm) over the sample with scanning angle ranging from 20 to 60°. The recorded XRD patterns of graphene nanoplatelets (GNP) and graphite is shown in **Figure 9**. One peak is appeared at 26.4° in graphite referring highly stacked structure with an interlayer spacing of 0.34 Å for graphite with a calculated particle size of approximately 145 nm by using Scherrer's formula [24]. This peak also appears inside GNP is referred to same graphite primitive plane (002) with a d-spacing of 3.37 Å. The intensity of the peak is very low as compared to graphite. This low intensity is due to the small number of layers present inside GNP with a thickness of ~1 nm and the calculated particle size was 35 nm which corresponds to 24 graphene sheet inside one GNP particle.

The XRD of C-series (BLFO/GNP and BLFMO/GNP) nanohybrids are shown in **Figure 10**. The labeled peak of BLFO (**Figure 10a**) are referred to as the primitive hkl planes (012), (104), (110), (006), (202), (024), (116), (112), (018) and (214) of bismuth ferrite BFO corresponding to the JCPDS card no. 20-0169. The perovskite rhomboidal structure of bismuth ferrite distort due to the addition of lanthanum due to which the intensity of peaks is reduced [25]. A small peak of an impurity $Bi_2Fe_4O_9$ is also appeared in BLFO/GNP which is not present inside BLFO/GNP with the introduction of graphene nanoplatelets. As these peaks in hybrid structure are broadened also with the decreased intensity which is representing the disorderedness introduced in hybrid structure with the addition of graphene sheets and hence, the low crystallinity. An extra peak also appeared in hybrid structure of hkl (002) plane which is a clear proof of formation of BLFO/GNP nanohybrid. With the introduction of manganese (5–25%) the Bi/Fe deficiencies were compensated and the impurity peak has been completely removed as the Mn amount was increased as shown in **Figure 10b–f**. The crystal structure of co-doped bismuth ferrite is transformed completely from rhombohedral to orthorhombic with the addition on Mn [26] and this is why the peaks are overlapped. As inter-planar spacing is inversely proportional to diffraction angle, a positive shift in peak was appeared up to Mn = 15% which showed a decrease in lattice constant. This decrement in lattice constant is due to the replacement of Fe with Mn-atoms which has a lower atomic radii than Fe [27]. With a further increase in Mn percentage (BLFMO-20 and BLFMO-25), negative peak shift is observed due to creation of compressive strain inside crystal structure. With the introduction of Mn in hybrid structure (BLFMO-5/GNP to BLFMO-25/GNP), there is a same trend of peak broadening and decreased intensity as was in BLFO/GNP representing complete incorporation of graphene layers inside BLFMO nanoparticles. The (002) peak of graphitic structure is also present showing graphene presence inside the nanohybrid. The particle sizes are also calculated by using Scherrer's formula [24] ranging from 19.3 to 23.5 nm. A small amount of impurity ($Bi_2Fe_4O_9$) is also present in BLFMO-25/GNP. There is more disorderedness in C-series nanohybrids crystal structure due to enhanced fusion of GNP sheets inside BLFO and BLFMO nanoparticles.

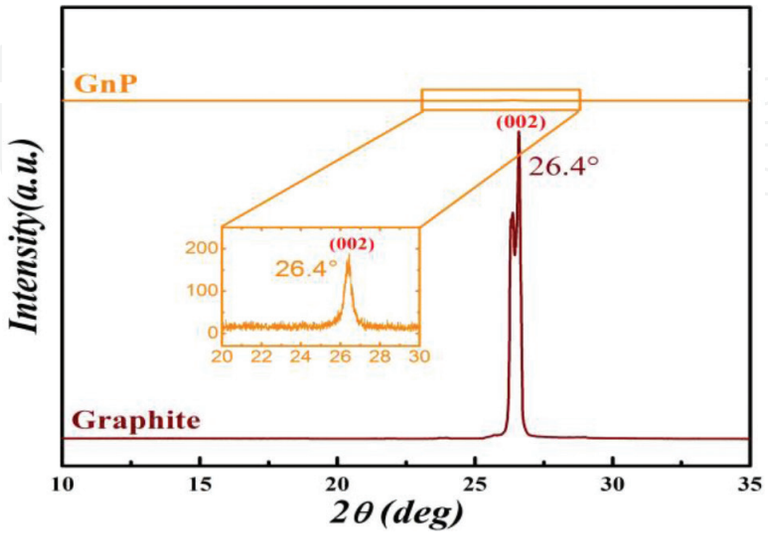

Figure 9. X-ray diffraction pattern of graphite (dark brown) and graphene nanoplatelets GNP (yellow).

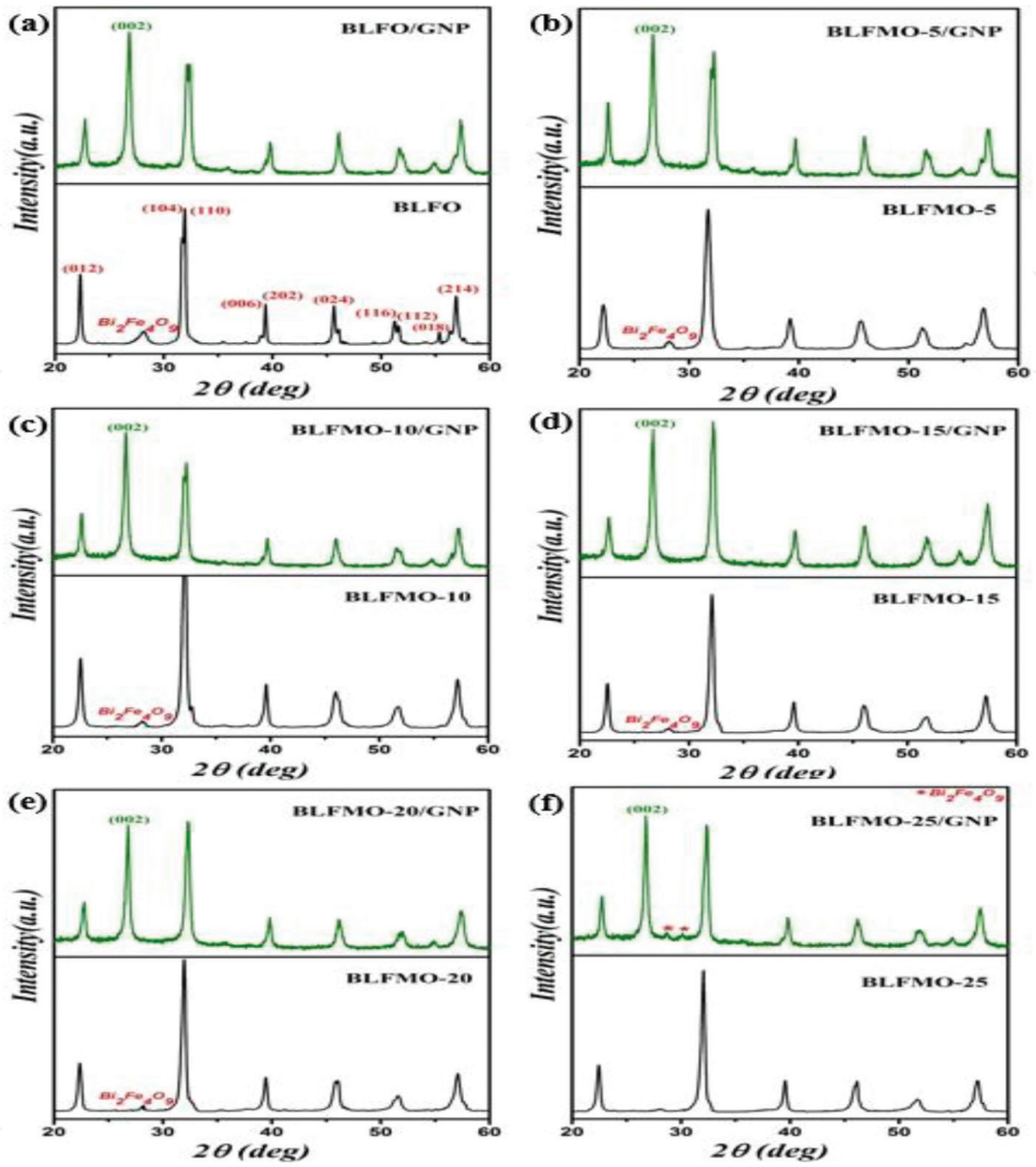

Figure 10. XRD patterns of C-series nanohybrids respectively as (a) BLFO/GNP, (b) BLFMO-5/GNP, (c) BLFMO-10/GNP, (d) BLFMO15/GNP, (e) BLFMO-20/GNP, (f) BLFMO-25/GNP.

3.2. C-series morphological analysis

Scanning electron microscope image of graphene nanoplatelets (GNP) is shown in **Figure 11**. Flat and smooth graphene sheets with sharp corners are clearly seen in SEM image. The commercial grade graphene layers (up to 24) are stacked together in the form of flakes inside GNP and are shown thick and darker in appearance.

Figure 12 shows the SEM micrographs of hybrid structures representing the mixed morphology of BLFO or BLFMO nanoparticles (white granular part) and graphene sheets (dark layered part). BLFO and BLFMO nanoparticles were not even attached with the edge atoms covalently but also adsorbed by the surface of graphene layers inside GNPs. The GNP consists of stacked

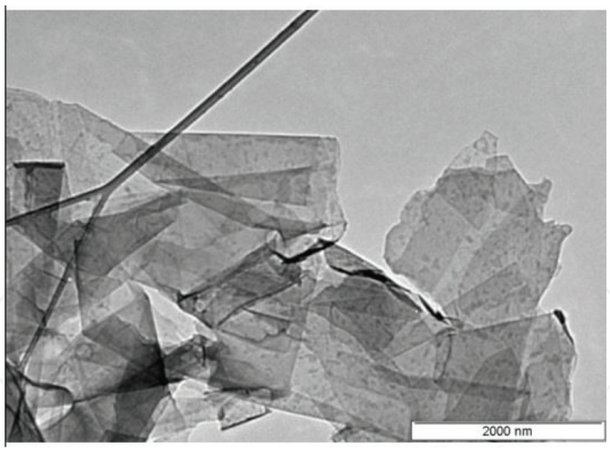

Figure 11. SEM image of graphene nanoplatelets (GNP) representing sheet structure of graphene.

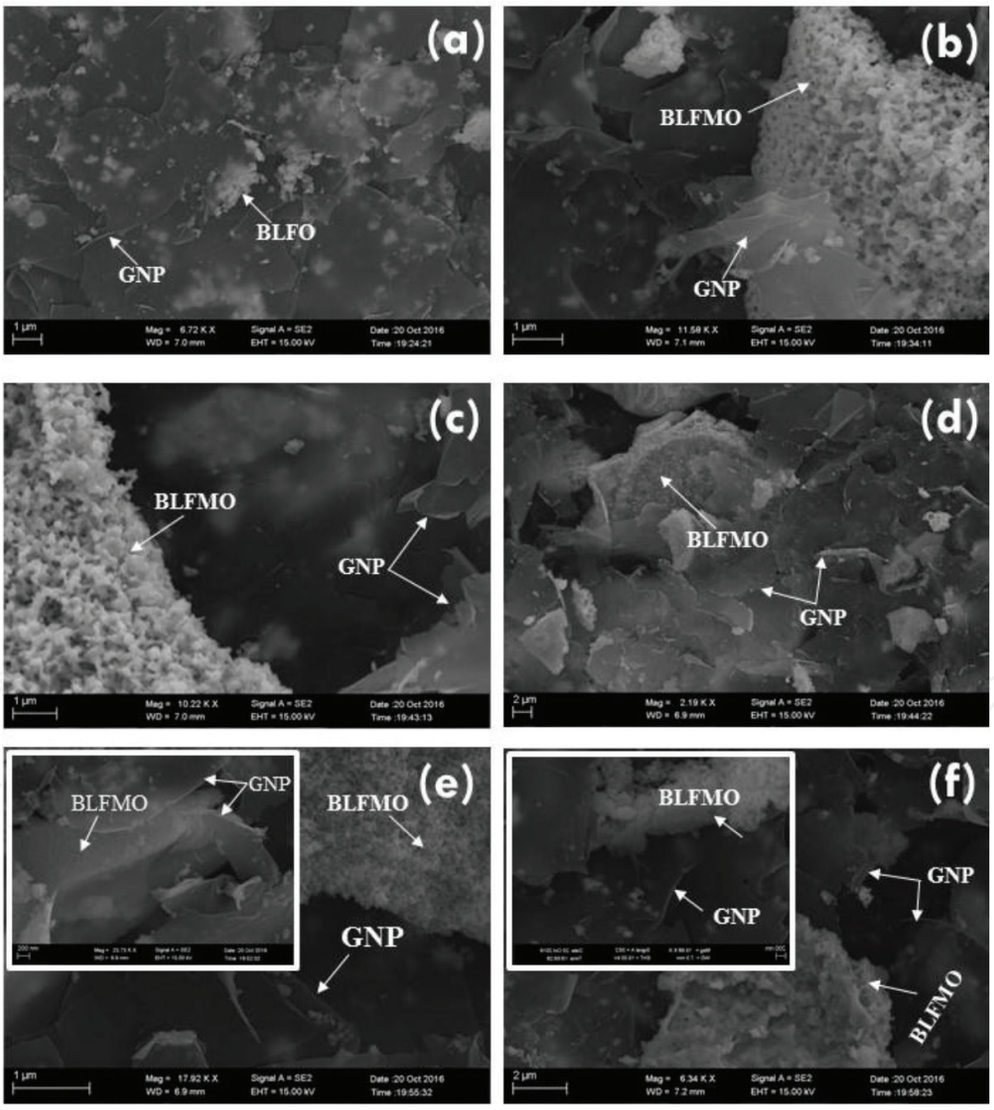

Figure 12. SEM micrographs of (a) BLFO/GNP, (b) BLFO-5/GNP, (c) BLFMO-10/GNP, (d) BLFMO-15/GNP, (e) BLFMO-20/GNP, (f) BLFMO25/GNP nanohybrids showing mixed morphology of both nanoparticles and graphene sheets; inset: shows big clusters of agglomerated particles.

graphene layers in the flake form and adsorbance of particles provides a sandwiched structure of layers in-between the nanoparticles. The particle adsorbancy gives an icy transparent effect to hybrid structures due to which the nanoparticles are clearly visible through the layers in SEM images. The rapid growth of particles over graphene layers provides a damage to the graphene sheets inside GNP resulting more disordered hybrid structures which is consistent with the XRD results. There is also an agglomeration of nanoparticles inside GNP and can be seen in the form of clusters of particles in SEM images.

The TEM micrographs are shown in **Figure 13** representing the BLFMO nanoparticles (dark part) and the light graphene sheets. Spherical BLFMO nanoparticles are not even connected to interface but are also distributed over the surface of graphene sheets in the form of small clusters. Due to overlapping of nanoparticles over the sheets, it is hard to distinguish a separate particle inside the hybrid structures. The estimated average particle size from the TEM micrographs using image-J software is ~ 31 nm.

3.3. X-ray photoluminescence of C-series

Figure 14 represents the X-ray Photoluminescence (XPS) spectra of C-series nanohybrids which helps in analyzing the detailed chemical composition of hybrid structures. The given peaks of bismuth (Bi), iron (Fe), lanthanum (La), manganese (Mn), oxygen (O) and carbon (C) at their corresponding binding energies of 159.1, 711, 837.5, 641.5, 529.8 and 284.7 eV are shown which are already reported before [28–30]. The main peaks verifying both the material's (BFO and graphene) elemental composition are also shown in **Figure 14b-d**. The Bi and O represents two peaks for Bi4f (**Figure 14b** and **c**) while C shows only one peak (**Figure 14d**) representing a network of C-C atoms. There are three main peaks in pristine GNP [31] which corresponds to C1s (a high intensity peak), O1s (a low intensity peak) and OKLL (oxygen vacancies created due to reduction process). The high intensity peak of Oxygen is due to the introduction of O atoms of BFO inside the hybrid material. There is no additional peak of other functional groups like C-H, COOR and C-O present inside BLFMO/GNP nanohybrid as they are eliminated during the reduction process of GNPs. There is peak of OKLL at 970 eV

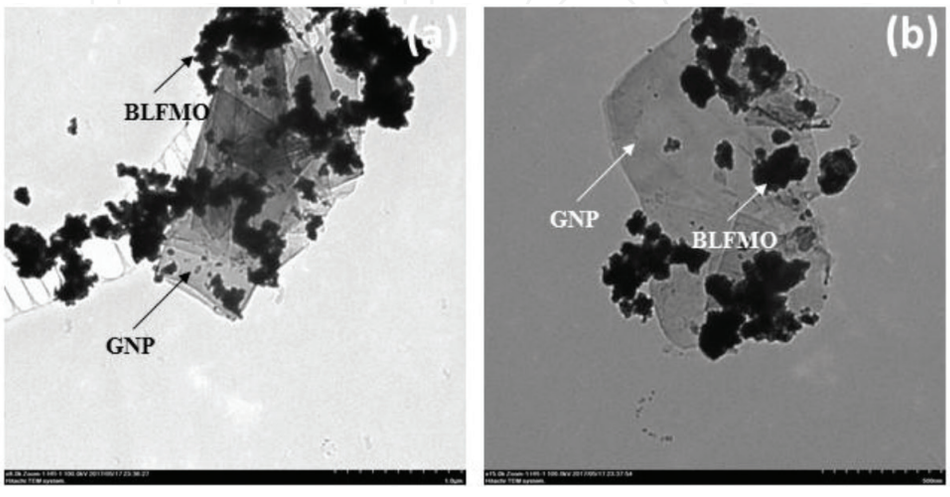

Figure 13. TEM images of BLFMO/GNP nanohybrids of C-series at (a) 1 μm and (b) 500 nm, resolution.

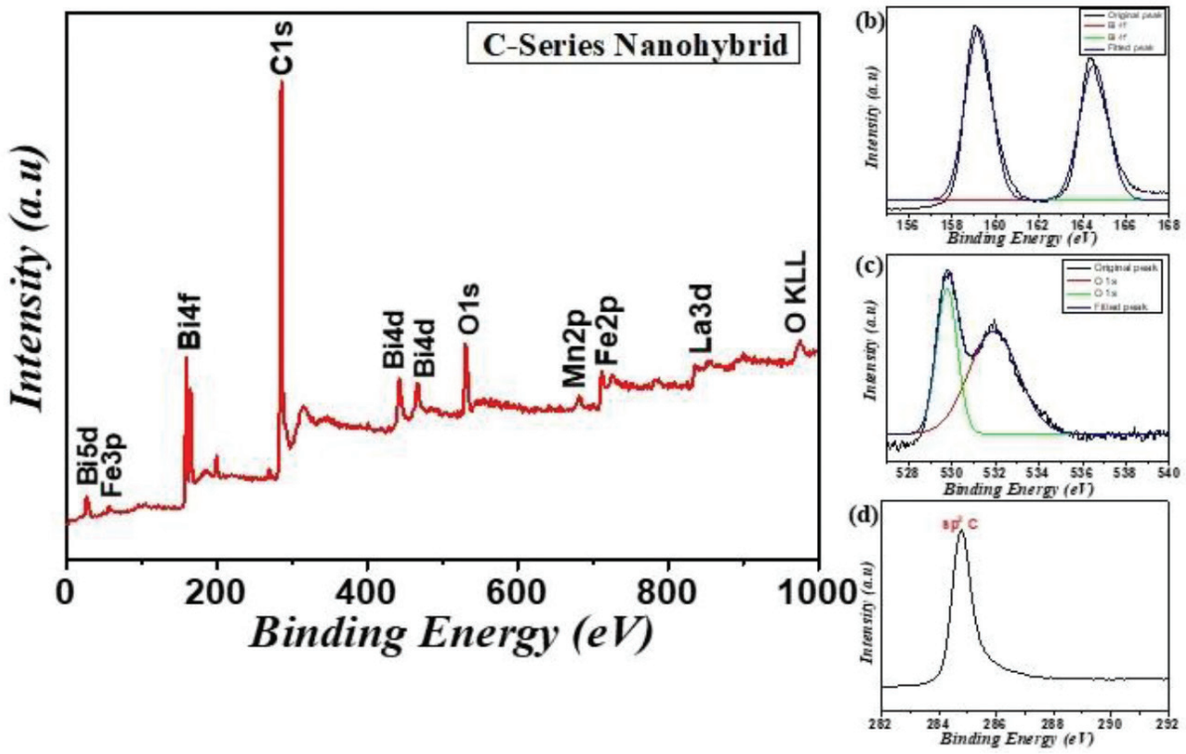

Figure 14. X-ray photoluminescence spectra of C-series nanohybrid.

which corresponds to both, GNP and BFO as oxygen vacancies are produced inside BFO during charge compensation and inside the graphene during reduction.

3.4. H-series structural analysis

The X-ray diffraction pattern of H-series nanohybrids is shown in **Figure 15**. The BLFO XRD pattern with its hybrid form of BLFO/GNP is shown in **Figure 14a**. All labeled peaks represent the bismuth ferrite (BFO) hkl planes (012), (104),(110), (006), (202), (024), (116), (112), (018) and (214), respectively. Peaks are broadened as compared to pure BFO which is due to the rhombohedral crystal structure distortion of BLFO with the introduction of Lanthanum. An impurity peak of $Bi_2Fe_4O_9$ is also appeared inside BLFO with the La addition which is disappeared in BLFO/GNP nanohybrid. The peaks inside the BLFO/GNP hybrid are broadened due to low periodicity in crystal structure with the incorporation of graphene sheets inside BLFO nanoparticles. An extra peak of (002) graphitic plane is also appeared in BLFO/GNP hybrid representing the successful fabrication of hybrid structure. The addition of manganese inside BLFO crystal structure is completely transformed from rhombohedral to orthorhombic and the overlapping of peaks is giving a clear proof of this transformation as shown in **Figure 16b-f**. The positive peak shift up to Mn = 15% is due to decrease of lattice constant as interlayer spacing is inversely related with the diffraction angle. The replacement of iron atoms with Mn-atoms causes the decrease in d-spacing because Mn have low atomic radii than iron. The impurity peak is first decreased and then disappeared with the increase amount of Mn (up to 25%) because of the compensation of bismuth-iron deficiencies. A negative peak shift is also occurred as Mn doping is increase above 15% which is due to the compressive strain produced

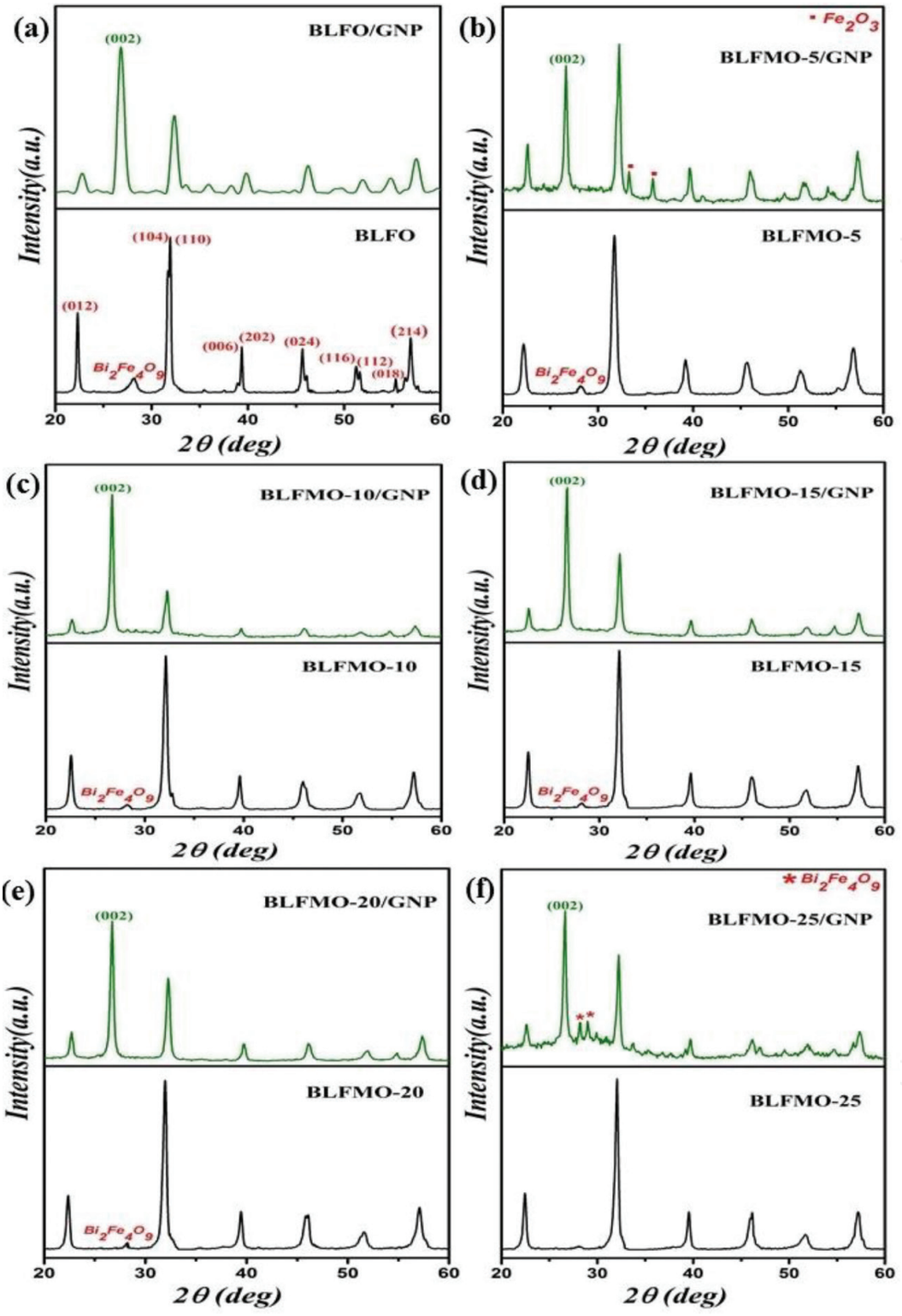

Figure 15. XRD patterns of H-series nanohybrids respectively (a) BLFO/GNP, (b) BLFMO-5/GNP, (c) BLFMO-10/GNP, (d) BLFMO15/GNP, (e) BLFMO-20/GNP, and (f) BLFMO-25/GNP.

inside the crystal structure. The broadening of peaks inside BLFMO-20 and BLFMO-25 is due to the surface defects and Mn-atoms trapped inside the crystals [32]. With the introduction of Mn atoms in hybrid structure from BLFMO-5/GNP to BLFMO-25/GNP, the peaks become

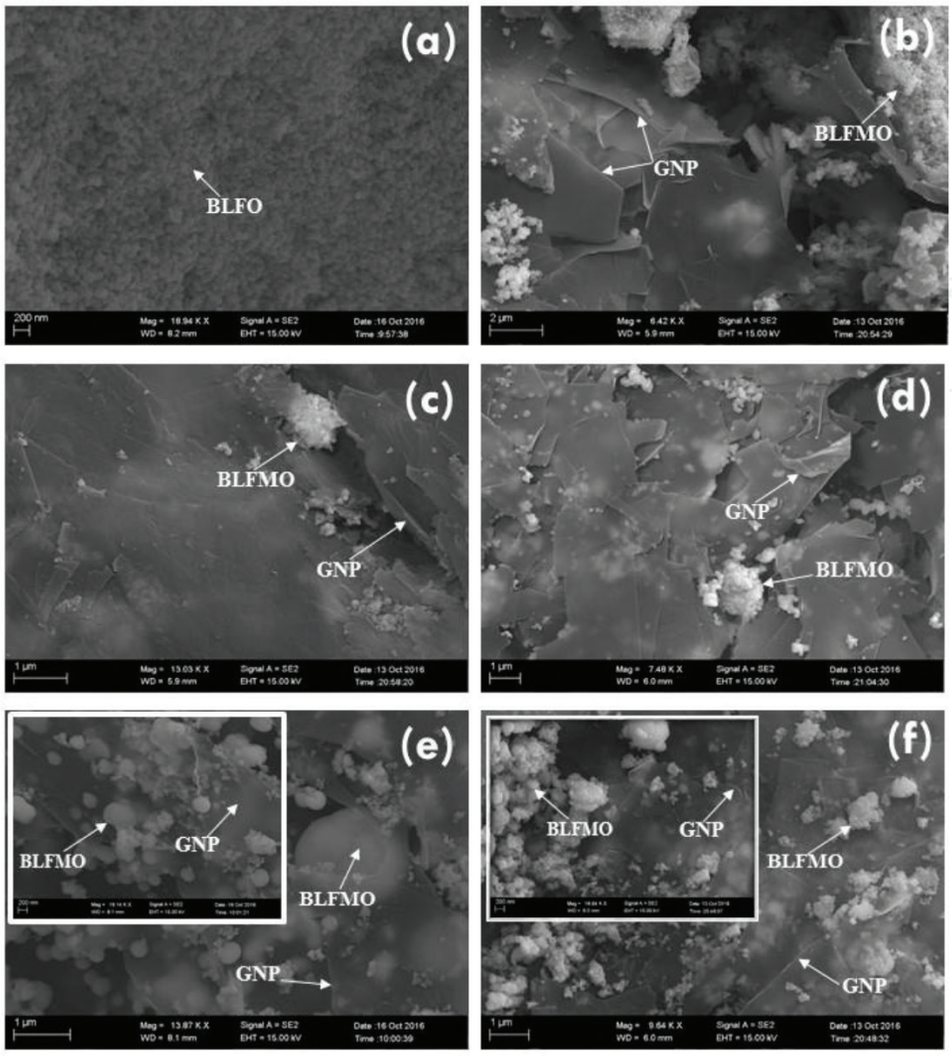

Figure 16. SEM micrographs of (a) BLFO/GNP, (b) BLFO-5/GNP, (c) BLFMO-10/GNP, (d) BLFMO-15/GNP, (e) BLFMO-20/GNP, (f) BLFMO25/GNP nanohybrids showing both, nanoparticles and graphene sheets morphology together. Inset: Uniform distribution of nanoparticles over graphene sheets.

more narrower and intensity of peaks is also increased which shows more crystallinity and periodicity inside the hybrid structure.

In hydrothermal method under controlled conditions of temperature and pressure, stable and good quality fine crystals can easily be grown with having a good control over hybrid composition. As the structure is more crystalline and ordered, small amount of impurities ($Bi_2Fe_4O_9$ and Fe_2O_3) are also appeared inside crystal structure of BLFMO/GNP nanohybrids. A positive shift in (002) peak is also observed inside the hybrid structures which can be occurred due to produced tensile strain with the introduction of uniformly distributed BLFO or BLFMO particles inside GNP layers [33]. The crystallite sizes are also calculated using Scherrer's formula which ranges from 22.5 to 26 nm.

3.5. H-series morphological analysis

Figure 16 shows SEM micrographs of H-series representing both, nanoparticle and sheet morphologies inside hybrid structures. In **Figure 16a**, the GNP sheets are not very much visible

as the whole surface of graphene sheets is covered with the adsorbed BLFO nanoparticles. As the GNPs are efficient nanofillers in nanohybrid synthesis and form a good dispersion, well dispersed and uniformly distributed BLFMO nanoparticles over the smooth surface of graphene nanoplatelets can be clearly seen in SEM images (**Figure 16b-f**).

Hydrothermal fabrication is a controlled growth synthesis process under high pressure and temperature conditions which enables graphene sheets to be more focused towards nucleation centers and thus, more uniform nanohybrids are formed. Mesoporous BLFMO particles are well embedded inside and over the graphene sheets inside GNP and are more visible in inset of SEM images. A transparency effect shown in SEM micrographs is due to the surface adsorption of BLFMO nanoparticles over graphene sheets. These sheets are stacked over one another inside GNP or in other words, are sandwiched in between the BLFMO nanoparticles which is why particles can be seen through the transparent graphene layers.

The H-series and C-series hybrids are further subjected to the photocatalytic experiments and measurement.

3.6. Photocatalytic activity

The photocatalytic activity is checked by measuring the degradation efficiency of hybrid structure in removal of the organic dye congo red (CR). The absorption spectra measured at a specific wavelength λ was compared with the maximum absorption at λ = 496 nm. The diffused reflectance spectra (DRS) of BLFO/GNP and BLFMO/GNP hybrids is shown in **Figure 17**. There is low optical absorption of hybrid structures in UV region as compared to the pure bismuth ferrite and then an overlap is occurred and optical absorption increases for the visible region (550 nm-700 nm). This increase in optical absorption enables the BLFMO/GNP nanohybrids as an efficient photocatalyst under visible light irradiation.

The optical absorption coefficient is related to the given Kubelka-Munk function (Eq. (1)) which is actually responsible for edge absorption.

$$(\alpha h\upsilon) = A\left(h\upsilon - E_g\right)^{n/2} \tag{1}$$

Here, Eg is bandgap energy, A and n are constants respectively, υ and h are light frequency and plank's constant [34].

Optical band gap of BLFO/GNP and BLFMO/GNP were also calculated by drawing a graph in between photon energy and $(\alpha h\upsilon)^2$ and are compared with the pure bismuth ferrite as shown in **Figure 18**. A straight line drawn over the $(\alpha h\upsilon)^2$ vs. energy plot till the point where it goes to zero provides the approximate band gap of hybrid structure. The obtained band gap of BLFMO-20/GNP hybrid structure is significantly reduced to 1.40 eV in comparison to BFO (2.04 eV). Here in all hybrid structures with small changes in optical absorption for visible range, it is slightly difficult to measure the onset of decreasing amount in optical absorption. A decrease in band gap illustrates that there are more chances of an efficient charge transfer and hence an enhanced photocatalytic activity.

The photocatalytic degradation efficiency of the hybrid structures was measured by checking the degradation rate of congo red organic dye under visible light. The obtained plots for

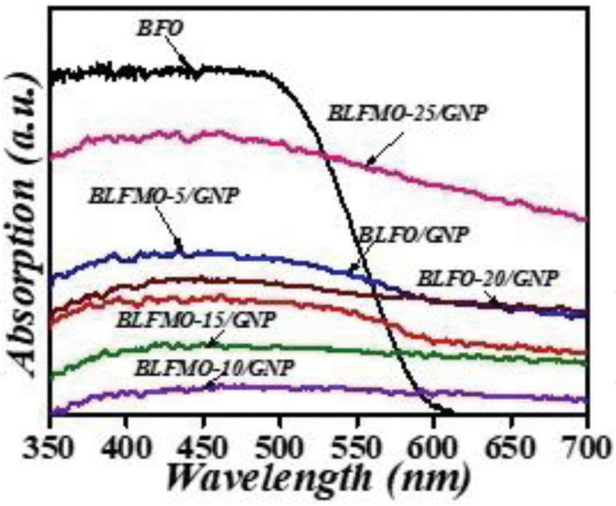

Figure 17. UV-visible absorption spectrum of pure BFO, BLFO/GNP and BLFMO/GNP hybrid structures.

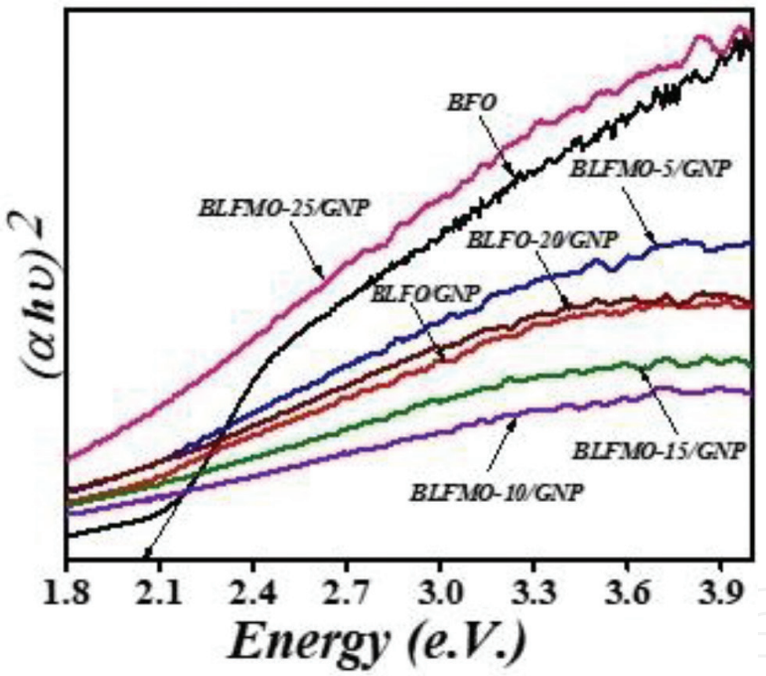

Figure 18. Measurement of the optical band gaps of the BFO, BLFO/GNP and BLFMO/GNP nanohybrids.

photocatalytic degradation are shown in **Figure 19**. The total photocatalytic degradation efficiency of pure BFO is 40% as shown in **Figure 19a** (H-series nanohybrids). The overall catalytic activity of H-series nanohybrids depends upon two factors: (i) adsorption of dye over material surface and (ii) degradation of dye under visible light irradiation. The surface adsorption of dye for BLFMO-15/GNP, BLFMO-20/GNP and BLFMO-25/GNP is 36, 65 and 54% while the photodegradation of dye is about 19, 11 and 9%, respectively. The total dye removal for BLFMO15/GNP, BLFMO-20/GNP and BLFMO-25/GNP nanohybrids is 55, 76 and 63%. C-series nanohybrids catalytic activity is shown in **Figure 19b**. The surface adsorption of dye for BLFO/GNP, BLFMO-5/GNP, BLFMO-15/GNP and BLFMO-25/GNP is 92, 70, 67 and 62% while the

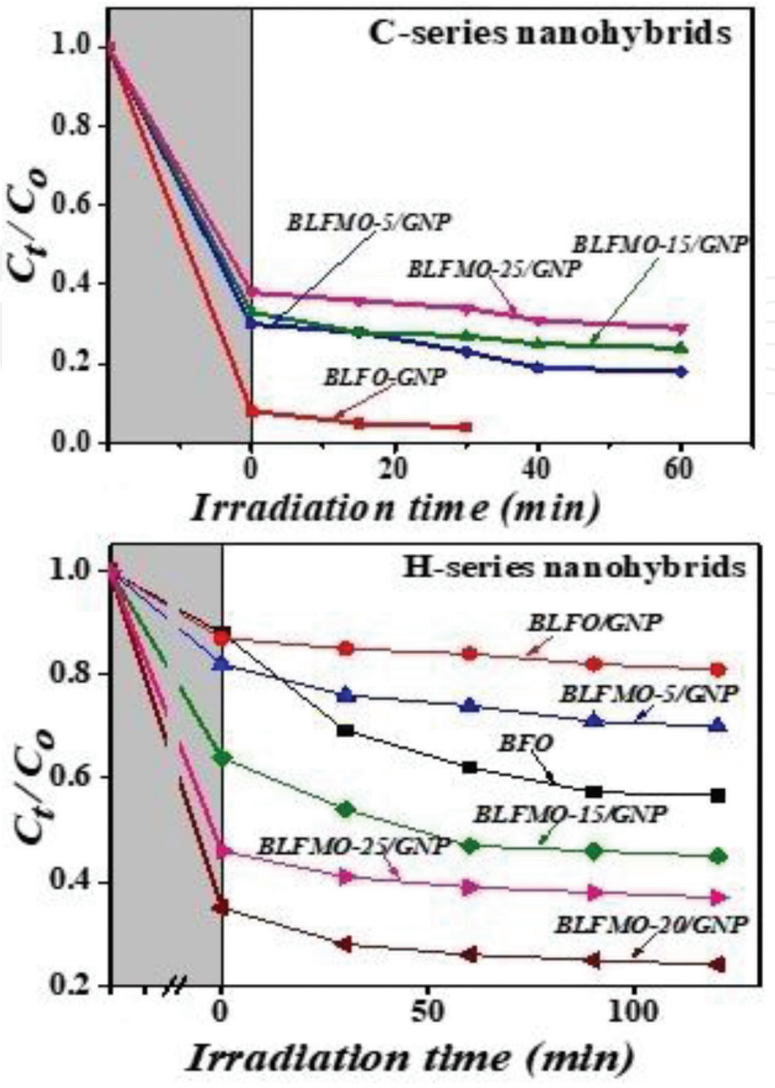

Figure 19. Photocatalytic efficiencies of BFO and BLFMO/GNP nanohybrids degrading the CR under visible light.

photo-degradation of dye is about 4, 12, 9 and 8%, respectively. The total dye removal for BLFO/GNP, BLFMO-5/GNP, BLFMO-15/GNP and BLFMO-25/GNP nanohybrids is 96, 82, 76 and 70%, respectively. The time taken by H-series hybrid structures to remove the whole dye from the aqueous solution was 120 min while it was 30 min for the C-series BLFO/GNP nanohybrid. The more dye removal due to surface adsorption is due to enhanced incorporation of GNP sheets inside BLFO nanoparticles. As co-ppt synthesis took more time for GNP sonication so there will be more yield of graphene due to exfoliation of sheets inside GNP. Graphene inclusion inside a nanohybrid helps in enhancing its specific surface area which causes more surface adsorption inside the material. In the following section, Brunauer Emmett Teller and photoluminescence measurement are performed to support the catalytic results.

3.7. Brunauer Emmett Teller measurements for C-series nanohybrid

To measure the specific surface area, BET measurement was performed and the obtained Nitrogen adsorption–desorption curve is shown in **Figure 20**. The observed curve is of type IV

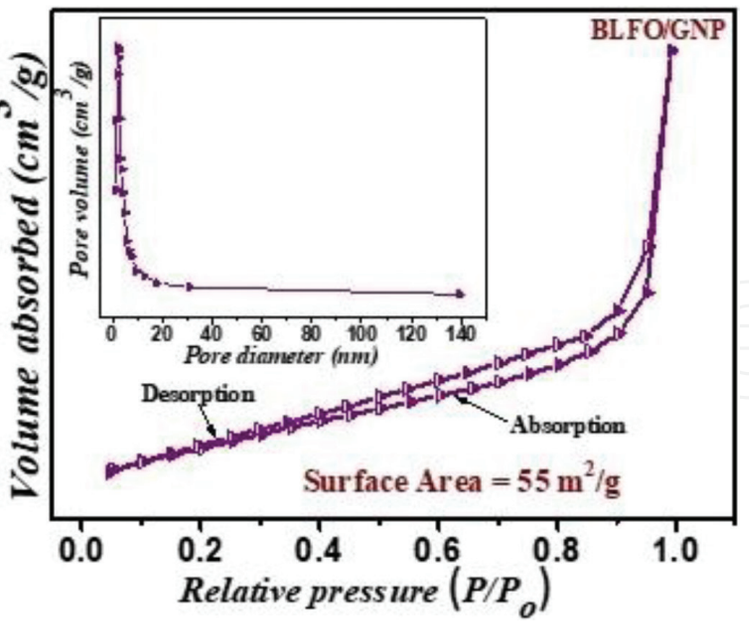

Figure 20. Nitrogen adsorption-desorption curve for surface area measurements of C-series BLFO/GNP nanohybrid.

(H3 hysteresis) with mesopore existence [35]. The average pore diameter and total pore volume for BLFO/GNP is 13.32 nm and 0.184 cm^3/g, respectively. The surface area of pristine BFO is 3.3 m^2/g [36] while the surface area for BLFO/GNP is enhanced up to 55 m^2/g due to the GNP loading inside BLFO nanoparticles. The enhanced surface area is representing the presence of multichannel structure inside BLFO/GNP nanohybrid which permits rapid mass movement and more intake of light harvesting due to increased absorption and multiple light reflections with gas diffusion inside the material's pores [37, 38]. The existence of mesopores with macro-channel structure attribute to more trapping of dye molecules over the material's surface Hence both adsorption over the surface and multiple light reflections together attribute in enhancing the photocatalytic activity of the nanohybrid which results in fast dye degradation.

3.8. Photoluminescence spectra of C-series nanohybrids

In photoluminescence measurement, electron-hole recombination rate is checked which promotes the efficient charge separation inside the photocatalytic material. The low PL intensity gives us low carrier recombination rate and hence, easily promotes the charge carriers over material surface for photo-degradation of dye [39]. The loading of graphene usually reduces the PL intensity due to graphene being a good trapping site for electrons and hence, easy charge transfer over catalyst surface [40]. **Figure 21** represents photoluminescence spectra of Pure BFO and C-series. Pristine BFO has larger band gap as compared to hybrid structures which is why the PL has high intensity for pure BFO showing more recombination rate The peak intensity is low for BLFMO-5/GNP and BLFMO-15/GNP as compared to BLFO/GNP and BLFMO-25/GNP. The low peak intensity refers to low recombination rate of charge carriers and hence more dye degradation under visible light. Hence, BLFMO-5/GNP (12%), BLFMO-15/GNP (9%) show more dye-degradation under visible light as compared to BLFO/GNP (4%) and BLFMO-25/GNP (8%).

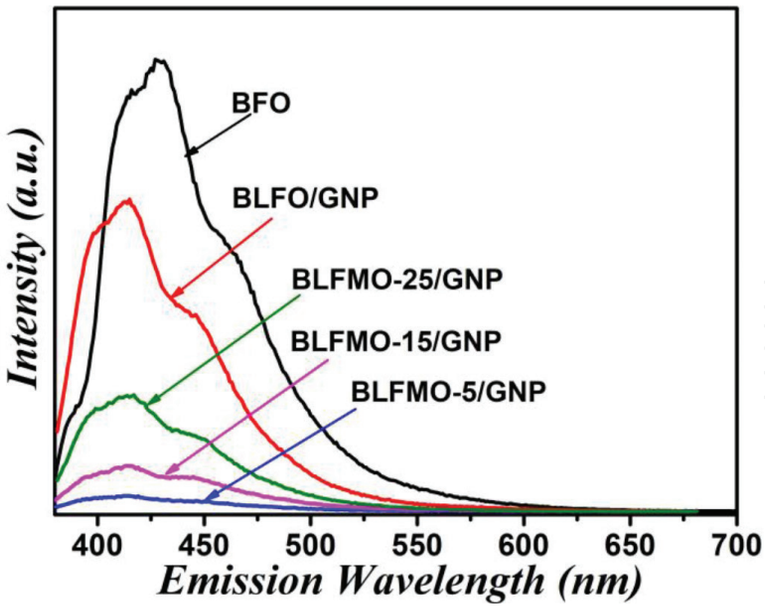

Figure 21. Photoluminescence spectra of C-series nanohybrids.

4. Conclusion

Here using sol-gel method lanthanum (La) and manganese (Mn) doped BFO nanoparticles were prepared and named as BLFO and BLFMO nanoparticles. These nanoparticles were further process to the coprecipitation and hydrothermal routes for synthesizing nanohybrids with graphene nanoplatelets (GNP). As synthesized BLFO/GNP and BLFMO/GNP nanohybrids via different routes were named as C and H series, respectively. Further nanohybrids were undergo structural and morphological analysis using XRD and SEM which show that the H-series nanohybrids are showing more crystallinity as compared to the C-series nanohybrids. The energy level introduced with the addition of Mn into BFO nanoparticles reduces the band-gap of nanohybrids. The detailed elemental composition of nanohybrids was checked using XPS which verified the bonding between nanoparticles and GNP. The BET shows that surface area is greatly enhanced from 3.3 m^2/g (for pure BFO) to 55 m^2/g (for C-series nanohybrid) which then contributes in fast dye removal as a result of both surface adsorption and photo-degradation. Hence C-series nanohybrids are more efficient as catalysts rather than H-series and showed 96% dye removal in only 30 min. The catalytic activity mainly depends upon the adsorption of dye over catalyst surface under dark conditions. These nanohybrids are very much applicable for commercial applications as they are fabricated via an easy and cost effective route and provide a fast and efficient dye removal from aqueous solution.

Acknowledgements

The authors are thankful to Higher Education Commission (HEC) of Pakistan for providing research funding under the Project No.: 6040/Federal/NRPU/R&D/HEC/2016 and

HEC/USAID for financial support under the Project No.: HEC/R&D/PAKUS/2017/783. The author also thanks School of Natural Sciences (SNS) at National University of Science & Technology (NUST), Islamabad, Pakistan for partial financial support.

Notes/thanks/other declarations

Special thanks to Dr. S. Irfan Ali at Tsinghua University, China for providing all technical assistance and guidance for the project.

Conflict of interest

I declare that there is no conflict of interest for the content added in this chapter.

Author details

Syed Rizwan* and Sabeen Fatima

*Address all correspondence to: syedrizwanh83@gmail.com

Department of Physics, School of Natural Sciences (SNS), National University of Sciences and Technology (NUST), Islamabad, Pakistan

References

[1] http://www.nature.com/nmat/journal/v11/n5/images_article/nmat3318-f2.jpg

[2] http://www.reade.com/images/product_images/ferrite_compounds/bismuth_ferrite_structure.jpg

[3] Zaleski M. Thermally stimulated processes related to photochromism of scandium doped sillenites. Journal of Applied Physics. 2000;**87**:4279-4284. DOI: 10.1063/1.373066

[4] Borse PH, Joshi UA, Ji SM, Jang JS, Jeong ED, Kim HG, Lee JS. Band gap tuning of lead-substituted $BaSnO_3$ for visible light photocatalysis. Applied Physics Letters. 2007; **90**:034103-034105. DOI: 10.1063/1.2430932

[5] Nippolainen E, Kamshilin AA, Prokofiev VV, Jaskelainen T. Combined formation of a self-pumped phase-conjugate mirror and spatial subharmonics in photorefractive sillenites. Applied Physics Letters. 2001;**78**:859-861. DOI: 10.1063/1.1344570

[6] Catalan G, Scott JF. Physics and applications of bismuth ferrite. Advanced Materials. 2009; **21**:2463-2485. DOI: 10.1002/adma.200802849

[7] Falkovsky LA. Optical properties of graphene. Journal of Physics: Conference Series. 2008;**129**:1-7

[8] Choi W, Lee JW. Graphene: Synthesis and Applications. USA: CRC Press; 2016. vii p. ISBN: 9781439861875. DOI: 10.1088/1742-6596/129/1/012004

[9] http://www.rsc.orgejNR2012c2nr30605kc2nr30605k-s1.gif

[10] Wolf EL. Applications of Graphene: An Overview. Dordrecht London: Springer Science & Business Media; 2014. 19 p. ISBN: 978-3-319-03946-6

[11] http://www.slideshare.net/NCSRCommunications/graphenemanchester-beyondthe-sticky-tape

[12] https://www.slideshare.net/BusinessGrowthHub/prof-ian-kinloch-presentation-graphene-week-25th-june

[13] Mertens R. The Graphene Handbook. lulu.com; 2016. 16 p. ISBN: 9781365707674

[14] Geng Y, Wang SJ, Kim JK. Preparation of graphite nanoplatelets and graphene sheets. Journal of Colloid and Interface Science. 2009;**336**:592-598. DOI: 10.1016/j.jcis.2009.04.005

[15] http://xgsciences.us/aboutxgnp.html

[16] Okpala C. C., "Nanocomposites—An overview", International Journal of Engineering Research and Development. 2013:17-23. ISSN: 2278-800X

[17] Adrian MTS, Sonia ACC. Advances in Carbon Nanostructures. Croatia, Europe: InTech; 2016. 3 p. DOI: 10.5772/61730

[18] Jing LQ, Zhou W, Tian GH, Fu HG. Surface tuning for oxide-based nanomaterials as efficient photocatalysts. Chemical Society Reviews. 2013;**42**:9509-9549. DOI: 10.1039/C3CS60176E

[19] Stengl V, Popelkova D, Vlacil P. TiO_2-graphene nanocomposite as high performance photo catalysts. Journal of Physical Chemistry C. 2011;**115**:25209-25218. DOI: 10.1021/jp207515z

[20] Liang YY, Wang HL, Casalongue HS, Chen Z, Dai HJ. TiO_2 nanocrystals grown on graphene as advanced photocatalytic hybrid materials. Nano Research. 2010;**3**:701-705. DOI: 10.1007/s12274-010-0033-5

[21] Gao F, Chen XY, Yin KB, Dong S, Ren ZF, Yuan F, Yu T, Liu JM. Visible-light photocatalytic properties of weak magnetic $BiFeO_3$ nanoparticles. Advanced Materials. 2007; **19**:2889-2892. DOI: 10.1002/adma.200602377

[22] An J, Zhu L, Wang N, Song Z, Yang Z, Du D, Tang H. Photo-Fenton like degradation of tetrabromobisphenol A with graphene single bond $BiFeO_3$ composite as a catalyst. Chemical Engineering Journal. 2013;**219**:225-237. DOI: 10.1016/j.cej.2013.01.013

[23] Li Z, Shen Y, Yang C, Lei Y, Guan Y, Lin Y, Liu D, Nana CW. Significant enhancement in the visible light photocatalytic properties of $BiFeO_3$-graphene nanohybrids. Journal of Materials Chemistry A. 2013;**1**:823-829. DOI: 10.1039/C2TA00141A

[24] Kaelble EF. Handbook of X-Rays. USA: McGraw-Hill Education; 1967

[25] Garciaa FG, Riccardi CS, Simoes AZ. Lanthanum doped $BiFeO_3$ powders: Syntheses and characterization. Journal of Alloys and Compounds. 2010;**501**:25-29. DOI: 10.1016/j.jallcom.2010.04.049

[26] Irfan S, Rizwan S, Shen Y, Tomovska R, Zulfiqar S, Sarwar MI, Nan CW. Mesoporous template-free gyroid-like nanostructures based on La and Mn co-doped bismuth ferrites with improved photocatalytic activity. RSC Advances. 2016;**6**:114183-114189. DOI: 10.1039/C6RA23674J

[27] Gupta S, Sharma A, Tomar M, Gupta V, Pal M, Guo R, Bhalla A. Piezoresponse force microscopy and vibrating sample magnetometer study of single phased Mn induced multiferroic $BiFeO_3$ thin film. Journal of Applied Physics. 2012;**111**:064110-064116. DOI: 10.1063/1.3699021

[28] Li Y, Sheng CM, Wang DW, Yuan J. High-efficiency and dynamic stable electromagnetic wave attenuation for La doped bismuth ferrite at elevated temperature and gigahertz frequency. RSC Advances. 2015;**5**:77184-77191. DOI: 10.1039/C5RA15458H

[29] Xu Q, Sheng Y, Khalid M, Cao Y, Wang Y, Qiu X, Zhang W, He M, Wang S, Zhou S, Li Q, Wu D, Zhai Y, Liu W, Wang P, Xu YB, Du J. Magnetic interactions in $BiFe_{0.5}Mn_{0.5}O_3$ films and $BiFeO_3/BiMnO_3$ superlattices. Scientific Reports. 2015;**5**:1-8. DOI: 10.1038/srep09093

[30] Wang F, Drzal LT, Qin Y, Huang Z. Effects of functionalized graphene nanoplatelets on the morphology and properties of epoxy resins. High Performance Polymers. 2015;**28**:1-11. DOI: 10.1177/0954008315588983

[31] Sun R, Yao H, Zhang HB, Li YWMY, Yu ZZ. Decoration of defect-free graphene nanoplatelets with alumina for thermally conductive and electrically insulating epoxy composites. Composites Science and Technology. 2016;**137**:1-9. DOI: 10.1016/j.compscitech.2016.10.017

[32] Arya GS, Negi NS. Effect of In and Mn co-doping on structural, magnetic and dielectric properties of $BiFeO_3$ nanoparticles. Journal of Physics D: Applied Physics. 2013;**46**:1-8. DOI: 10.1088/0022-3727/46/9/095004

[33] Qiu B, Zhou Y, Ma Y, Yang X, Sheng W, Xing M, Zhang J. Facile synthesis of the Ti^{3+} self-doped TiO_2-graphene nanosheet composites with enhanced photocatalysis. Scientific Reports. 2015;**5**:1-6. DOI: 10.1038/srep08591

[34] Kubelka P, Munk F. Ein beitrag zur optik der farbanstriche. Technical Physics. 1931; **12**:593-601

[35] Chieng BW, Ibrahim NA, Yunus WMZW, Hussein MZ, Silverajah VSG. Graphene nanoplatelets as novel reinforcement filler in poly(lactic acid)/epoxidized palm oil green nanocomposites: Mechanical properties. International Journal of Molecular Sciences. 2012;**13**:10920-10934. DOI: 10.3390/ijms130910920

[36] Irfan S, Rizwan S, Shen Y, Liangliang L, Asfandiyar, Butt S, Nan CW. The gadolinium (Gd^{3+}) and Tin (Sn^{4+}) co-doped BiFeO3 nanoparticles as new solar light active Photocatalyst, Scientific Reports, 2017;**7**:1-12. DOI:10.1038/srep42493

[37] Zhao T, Liu Z, Nakata K, Nishimoto S, Murakami T, Zhao Y, Jiang L, Fujishima A. Multichannel TiO_2 hollow fibers with enhanced photocatalytic activity. Journal of Materials Chemistry. 2010;**20**:5095-5099. DOI: 10.1039/C0JM00484G

[38] Fang B, Bonakdarpour A, Reilly K, Xing Y, Taghipour F, Wilkinson DP. Large-scale synthesis of TiO_2 microspheres with hierarchical nanostructure for highly efficient photodriven reduction of CO_2 to CH_4. ACS Applied Materials & Interfaces. 2014;**6**:15488-15498. DOI: 10.1021/am504128t

[39] Arshad A, Iqbal J, Siddiq M, Mansoor Q, Ismail M, Mehmood F, Ajmal M, Abid Z. Graphene nanoplatelets induced tailoring in photocatalytic activity and antibacterial characteristics of MgO/graphene nnanoplatelets nanocomposites. Journal of Applied Physics. 2017;**121**:1-10. DOI: 10.1063/1.4972970

[40] Worajittiphon P, Pingmunag K, Inceesungvorn B, Phanichphant S. Enhancing the photocatalytic activity of ZnO nanoparticles for efficient rhodamine B degradation by functionalized graphene nanoplatelets. Ceramics International. 2015;**41**:1885-1889. DOI: 10.1016/j.ceramint.2014.09.023